

Evaluation of Hurricane Ocean Vector Winds From WindSat

Ian S. Adams, *Student Member, IEEE*, Christopher C. Hennon, W. Linwood Jones, *Fellow, IEEE*, and Khalil A. Ahmad, *Student Member, IEEE*

Abstract—The ability to accurately measure ocean surface wind vectors from space in all weather conditions is important in many scientific and operational usages. One highly desirable application of satellite-based wind vector retrievals is to provide realistic estimates of tropical cyclone intensity for hurricane monitoring. Historically, the extreme environmental conditions in tropical cyclones (TCs) have been a challenge to traditional space-based wind vector sensing provided by microwave scatterometers. With the advent of passive microwave polarimetry, an alternate tool for estimating surface wind conditions in the TC has become available. This paper evaluates the WindSat polarimetric radiometer's ability to accurately sense winds within TCs. Three anecdotal cases studies are presented from the 2003 Atlantic Hurricane season. Independent surface wind estimates from aircraft flights and other platforms are used to provide surface wind fields for comparison to WindSat retrievals. Results of a subjective comparison of wind flow patterns are presented as well as quantitative statistics for point location comparisons of wind speed and direction.

Index Terms—Hurricane, ocean vector wind, passive microwave polarimetry, tropical cyclone (TC), WindSat.

I. INTRODUCTION

THE measurement of global ocean surface wind vector (wind speed and direction), using microwave remote sensing techniques from polar orbiting satellites, provides vital environmental information for both scientific and operational applications. From a scientific standpoint, ocean vector wind data are critical to support basic research in global climate change, air-sea interaction, ocean and atmospheric circulation, and a variety of meteorological and oceanographic research topics. Operationally, these data are essential for short-term weather and ocean wave forecasts/warnings, ship routing, marine operations, hurricane analysis, etc. Also there are significant military applications of the wind vector, which affects a broad range of naval operations including strategic ship movement and positioning, aircraft carrier operations, aircraft deployment, underway replenishment, and littoral operations.

Manuscript received February 1, 2005; revised October 7, 2005. This work was supported by the Naval Research Laboratory WindSat Calibration/Validation Program.

I. S. Adams was with the Electrical and Computer Engineering Department, University of Central Florida, Orlando, FL 32816 USA. He is now with the Remote Sensing Division, Naval Research Laboratory, Washington, DC 20375 USA (e-mail: ian.adams@nrl.navy.mil).

C. C. Hennon was with the University Corporation for Atmospheric Research, Tropical Prediction Center, Miami, FL 33165 USA. He is now with the University of North Carolina-Asheville, Asheville, NC 28804 USA.

W. L. Jones and K. A. Ahmad are with the Electrical and Computer Engineering Department, University of Central Florida, Orlando, FL 32816 USA (e-mail: ljones5@cfl.rr.com).

Digital Object Identifier 10.1109/TGRS.2005.862506

Historically, the use of radar scatterometers on spacecraft to measure the ocean surface wind vectors is well established, with over 35 years of research and development [1]. Spaceborne scatterometers, such as the National Aeronautics and Space Administration's (NASA) NSCAT and SeaWinds instruments and the European Space Agency's Active Microwave Instrument on the European Remote Sensing 1 and 2 satellites, have observed global ocean winds continuously since the early 1990s. However, there have never been a sufficient number of these sensors simultaneously operational, in the proper orbits, to satisfy the revisit and coverage requirements necessary for full utilization in operational meteorological applications. At best, scatterometers observe ~90% of the ice-free oceans daily with a revisit time that ranges from 12–24 h, which is far from desired temporal sampling.

Further, the use of satellite passive microwave radiometry also has a strong heritage for remote sensing of atmospheric and oceanic environmental parameters. Over the past 15 years, a series of seven Special Sensor Microwave/Imagers (SSM/Is) has successfully operated on the Defense Meteorological Satellite Program (DMSP) satellites. Typically, there are two or more SSM/Is operating simultaneously in morning and evening sun-synchronous orbits. They have provided reliable passive microwave data for retrieving atmospheric and ocean environmental parameters such as integrated atmospheric water vapor and cloud liquid water, ocean surface wind speed, and sea ice concentration and type [2], [3]. Historically, the ocean surface wind direction is one parameter that has not been provided by microwave radiometers; however, analysis of SSM/I data has revealed a wind direction dependence (anisotropy) in the polarized ocean brightness temperatures, which has been confirmed by modeling and aircraft measurements [4], [5]. These empirical observations have provided the motivation for the WindSat experiment.

WindSat is the world's first passive microwave polarimetric radiometer. It was launched on the polar, sun-synchronous, low Earth orbit satellite Coriolis in January 2003. The objective of WindSat is to demonstrate the "proof of concept" of a new microwave polarimetric radiometry technique for measuring the ocean surface wind vector (speed and *direction*) from space. A significant part of this new research has been the definition of the wind direction signatures and the associated retrieval algorithm [6]–[8]. In late 2004, the first preliminary oceanic wind vector results (environmental data records version 1.5.1) were released to the science community. One important potential application for WindSat wind vectors is tropical cyclone (TC) analysis. Since TCs form and spend most of their lifetime

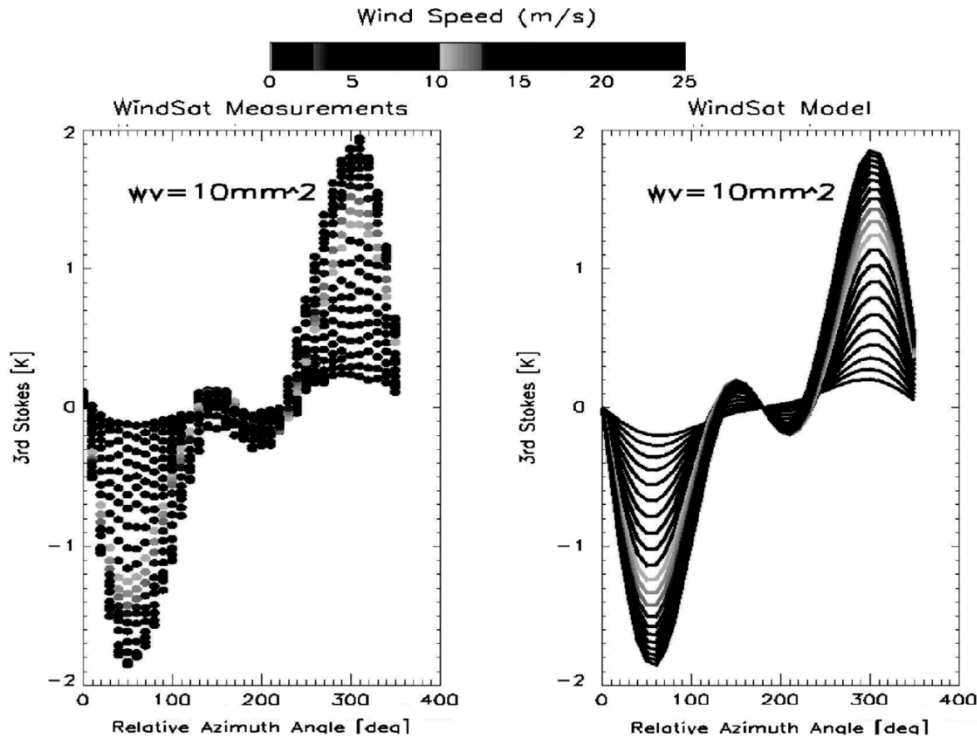


Fig. 1. Example of measured and modeled third Stokes wind direction geophysical model function at 18.7 GHz from [6].

over the data-poor oceans, surface wind vector data can make a vital contribution to identifying surface circulations and determining maximum surface wind speeds and radii. SeaWinds scatterometer data have been used at TC forecast centers worldwide for several years with some success. Unfortunately, SeaWinds retrievals experience a dramatic loss in accuracy in the presence of moderate and heavy rainfall and for high wind speeds [9]–[11]—common conditions in TCs. Thus, our primary motivation for this paper is to provide a preliminary assessment on alternative passive WindSat surface wind vector retrievals in TC environments. The hope is that WindSat will offer an additional dataset to operational forecasters, especially in determining the radii of gale force winds and possibly storm force and hurricane force winds.

This paper provides a brief description of the WindSat Project’s National Oceanographic and Atmospheric Administration (NOAA) National Environmental Satellite, Data, and Information Service (NESDIS) version-0 wind retrieval algorithm [7] and presents unique evaluations of wind vector retrievals in the high cloud liquid water/precipitation environment of a hurricane. Both wind speed and wind direction comparisons are made with an experimental tool known as H*Wind that performs surface wind analyses given a large of amount of heterogeneous data. To complement this surface wind analysis, rain rates are derived using WindSat brightness temperatures with a modified version of the TMI 2A12 heritage rain algorithm. Effects of rain on the derived wind speeds and directions are discussed.

Because WindSat is a proof-of-concept mission for the passive microwave measurement of wind direction, we feel the proper question to answer is “Do any WindSat retrieved direction aliases agree closely with the surface wind direction anal-

ysis?” Thus, the objective of this paper is to evaluate the ability of WindSat to retrieve realistic wind directions and to assess the suitability of the present geophysical model function in a tropical cyclone environment.

II. OCEANIC WIND VECTOR RADIOMETER POLARIMETRIC SIGNATURES

The microwave ocean brightness temperature (T_b) observed by a satellite radiometer depends upon a number of ocean surface and atmospheric geophysical variables, as well as measurement geometry. Fortunately, these T_b signatures are functions of the observing radiometer frequency (wavelength) and polarization, which permits the separation of these effects during the multifrequency radiometer geophysical retrieval process [12]. For this paper, we are only concerned with the T_b signatures for the ocean surface wind vector, which will be described next in very simplified terms.

As discussed in Gaiser *et al.* [13], recent advances in polarimetric radiometry modeling and measurements have demonstrated that usable wind direction information can be obtained by combining the vertical and horizontal polarizations with the cross-correlation of the two [14]–[19]. The cross correlation terms represent the third and fourth parameters of the modified Stokes vector [20], defined as

$$I_s = \begin{bmatrix} I \\ Q \\ U \\ V \end{bmatrix} = \begin{bmatrix} T_v \\ T_h \\ T_{45} - T_{-45} \\ T_{lc} - T_{rc} \end{bmatrix} = \begin{bmatrix} \langle E_v E_v^* \rangle \\ \langle E_h E_h^* \rangle \\ 2\text{Re} \langle E_v E_h^* \rangle \\ 2\text{Im} \langle E_v E_h^* \rangle \end{bmatrix}. \quad (1)$$

In this definition, T_v , T_h , T_{45} , T_{-45} , T_{lc} , and T_{rc} represent brightness temperatures (radiance) at vertical, horizontal, plus 45°, minus 45°, left-hand circular, and right-hand circular po-

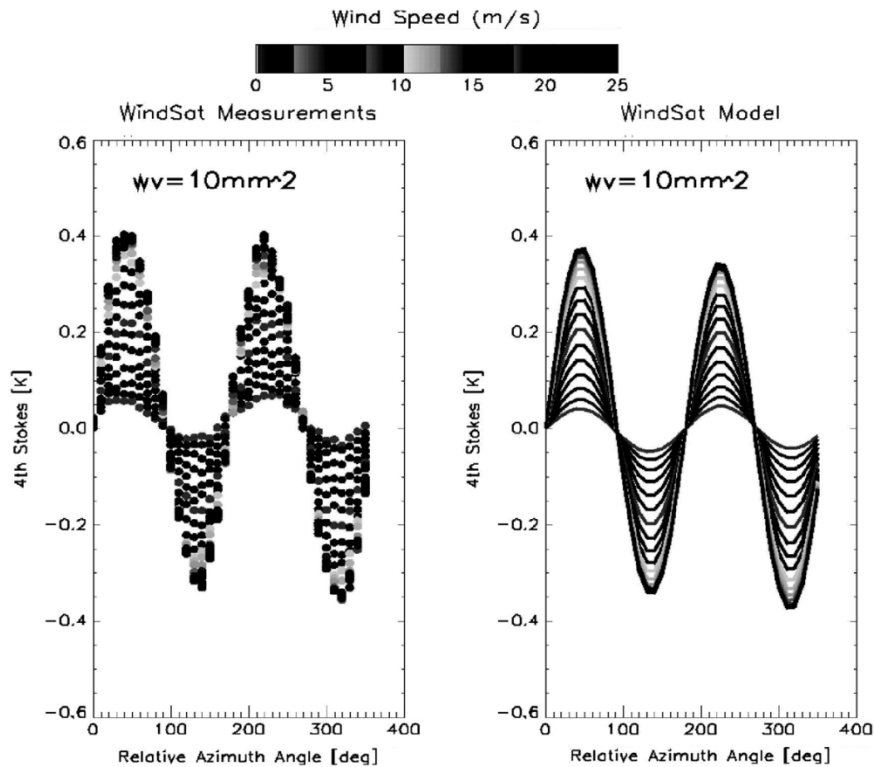


Fig. 2. Example of measured and modeled fourth Stokes wind direction geophysical model function at 18.7 GHz from [6].

larizations, respectively. In principle, the Stokes vector provides a full characterization of the electromagnetic signature of the ocean surface, which is sufficient to uniquely determine the wind direction.

Of these Stokes parameters, the most useful for wind direction measurement are the third (implemented by the difference between the $\pm 45^\circ$ polarization channels) and the fourth (implemented by the difference between the left- and right-hand circular polarization channels). On WindSat, there are three channels, 10.7, 18.7, and 37 GHz, that make polarimetric measurements. An example of the 18.7-GHz third Stokes signature, known as the geophysical model function (GMF), versus wind speed and direction is given in Fig. 1 [6]. From this figure, it is shown that the third Stokes parameter is anisotropic with the relative wind direction. This relative wind direction is defined as the difference between the wind direction and the azimuth-look of the radiometer antenna, where a relative azimuth equal zero corresponds to the wind blowing toward the radiometer antenna. The third Stokes can be modeled as a Fourier series of relative wind direction where the dc Fourier term is zero, and the anisotropic signature is predominantly the sum of the first and second harmonics, the coefficients of which are functions of wind speed.

The fourth Stokes parameter, shown in Fig. 2, is also anisotropic with relative wind direction. This parameter is basically second harmonic with a small first harmonic component, both of which have amplitudes which increase with wind speed. Both the third and fourth Stokes signatures are relatively weak as environmental radiometric signals go; but, fortunately, they are very robust in that they are highly immune to the influences of atmospheric absorption and emission caused by water

vapor and cloud liquid water. These atmospheric signals are common-mode and cancel during the subtraction of the $\pm 45^\circ$ and left- and right-hand circular polarizations. Unfortunately, the effect of heterogeneous precipitation is less certain because there are an extremely limited number of observations of the third and fourth Stokes parameters in the presence of rain. This may have influenced the evaluation results presented herein for hurricane wind direction measurements, which usually are accompanied by strong bands of precipitation. This will be discussed further in the following section.

III. WINDSAT WIND VECTOR RETRIEVAL

To aid in the understanding of the wind vector evaluation results presented later, a brief description of the NOAA/NESDIS version-0 WindSat wind vector retrieval algorithm [7] is discussed in this section, and a simplified flowchart presented in Fig. 3. The first step in the wind retrieval process is to process the four-frequency, vertically and horizontally polarized WindSat Tbs to determine cloud liquid water, water vapor, wind speed, and sea-surface temperature. These parameters are retrieved using a multivariate regression analysis, where the coefficients are derived from match-ups with buoys, ships, other satellites, and data assimilation models [8]. After solving for the four parameters, the entire process is repeated several times until the retrievals converge to a stable value. It should be noted that this environmental retrieval algorithm is not developed for winds above 20 m/s, nor is it developed for any environmental retrievals in rain, since the data chosen for the algorithm training set excluded any environmental parameters that contained rain or wind above 20 m/s.

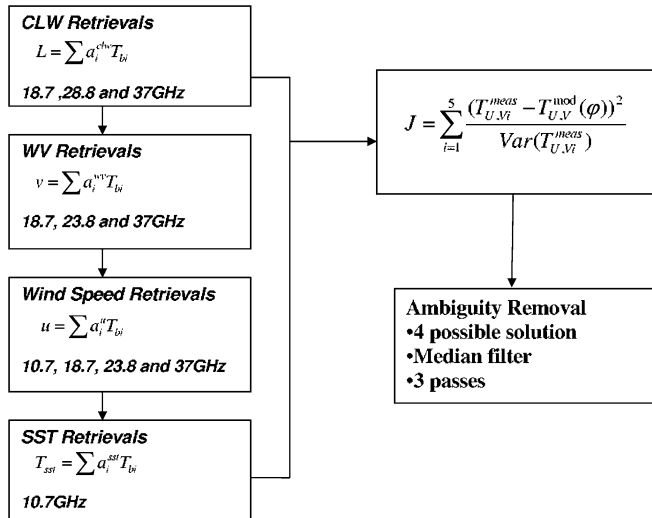


Fig. 3. NOAA NESDIS wind vector retrieval algorithm version-0 flowchart.

For the wind direction retrieval, the third and fourth Stokes parameters for the 10.7-, 18.7-, and 37-GHz polarimetric channels are used as inputs with the wind speed retrieved above and an atmospheric transmittance characterization for the third and fourth Stokes parameters derived from radiative transfer calculations. Relative wind directions are varied and the modeled third and fourth Stokes parameters, $(T_{U,V})^{\text{mod}}$, calculated. For each relative wind direction trial, the square of the difference between the measured and the modeled parameters $\{(T_{U,V})^{\text{meas}}$, and $(T_{U,V})^{\text{mod}}\}$ are calculated and summed for all frequencies. Values of relative wind direction that minimized the sum of these terms (cost function) for all frequencies were outputted as “possible solutions.” Because of the harmonic nature of the geophysical model functions (Figs. 1 and 2), multiple possible wind directions (called wind direction aliases) can result.

For microwave scatterometer wind direction retrievals, the retrieval process is similar; but because of differences in the radar backscatter GMF, the distribution of aliases is much different than that for passive microwave polarimetry. For scatterometer wind retrievals, the number of aliases range from two to four with the two most probable directions being roughly 180° apart. For WindSat, however, the most frequent number of aliases is two or three, and the directional differenced of aliases are rarely 180° apart. These WindSat aliases are ranked by the “goodness of fit,” which is proportional to the inverse of the cost function. After ranking, the aliases subjected to a multipass median filter to produce a single selected vector. The alias selection skill, which is defined as the percentage of the selected directions that are closest to the true direction, is quite high (typically $> 85\%$ for TCs).

IV. SURFACE WIND ANALYSIS (H*WIND)

As mentioned previously, verification of TC surface wind fields are inherently challenging due to the dearth of data available for these systems. Fortunately, estimates of TC wind fields are possible when reconnaissance aircraft fly missions through the storm. Since the 1990s, these data have been processed through the H*Wind [21] analysis system. H*Wind provides an objective analysis of the (TC) 1-min sustained-wind wind field

at a 10-m reference height by assimilating all available surface observations, as well as aircraft and remotely sensed data, into a common framework that also allows for limited human quality control. The H*Wind algorithms, graphical user interface, and databases were developed over a number of years at the NOAA Hurricane Research Division (HRD) and have been used for poststorm analysis and to experimentally support operational TC analysis. All data included in an analysis are transformed into a storm-relative coordinate system. In this paper, the storm centers are linearly interpolated from the surrounding “best track” fixes from the National Hurricane Center (NHC). Typical data sources for an H*Wind analysis include aircraft reconnaissance (flight-level winds (700 mb, or ~ 3000 m for both cases) reduced to a surface value, stepped-frequency microwave radiometer (SFMR) [22], QuikSCAT, SSM/I, buoys, ship reports, Geostationary Operational Environmental Satellite (GOES) low-level cloud drift winds [23], and global positioning satellite (GPS) dropwindsondes from aircraft [24].

A. Wind Speed Validation Set

Caution has to be used when applying an H*Wind analysis for wind speed validation purposes. There are three principal factors that introduce error into an analysis. First, H*Wind is not a snapshot of the wind field; rather, it is an assimilation of observations that have been collected during a 3- to 6-h period of observations. Furthermore, much of the storm circulation remains unobserved even by including data over such a time window. This produces a large degree of uncertainty in areas of the storm that were not sufficiently covered with observations. Second, there are instrument and processing errors from the observations that go into each analysis. In general, platforms that are designed to measure a 10-m wind (e.g., QuikSCAT, SFMR) have less error than those where a reduction factor or some other adjustment must be made (e.g., AFRES, GOES). Standard reduction factors do not take into account the varying stability profiles present throughout TCs. Of course there are important exceptions. For example, AFRES surface wind speeds are considered more reliable than buoy measurements in TCs, since buoys tend to underestimate surface wind speeds in troughs of large waves. Typical errors are: 1) buoys $\sim 10\%$ [26]; 2) QuikSCAT 5% (nonraining) [25]; 3) AFRES 10% (www.ndbc.noaa.gov), SFMR 10% to 15% [22]; and 4) GOES low-level cloud drift winds $\sim 10\%$ [23]. Third, the wind field structure of a typical TC is highly variable in both space and time. Since observations are taken over a long temporal window, it is almost certain that significant changes in the TC wind field have occurred, and thus a significant error range in the analysis field is introduced. Typical wind speed errors in an H*Wind analysis are estimated to be 10% to 20% [27], although that will vary depending on the quantity and quality of data that are available as well as the degree of quality control employed by the analyst.

In this paper, we were careful to choose two cases, where the TC was well sampled around the WindSat pass time, out of the possible six partial or complete WindSat passes over Atlantic TCs during the six-month data window. We selected Fabian (September 3, 2147 UTC) and Isabel (September 17, 1129 UTC) as suitable candidates for a wind speed comparison. In Table I, the times of the WindSat passes are shown along with the observations incorporated into each H*Wind analysis.

TABLE I
OBSERVATION PLATFORMS USED BY H*WIND TO PRODUCE THE
ANALYSES FIELDS FOR FABIAN AND ISABEL (2003)

Observation	Fabian 3 Sep. 2003 2147 UTC		Isabel 17 Sep. 2003 1129 UTC	
	Num Obs	Time Frame	Num Obs	Time Frame
AFRES	134	18:00 – 20:22	512	07:57 – 14:47
SFMR	701	18:00 – 23:20	0	
Moored Buoy	0		207	07:59 – 14:49
Drifting Buoy	12	18:00 – 00:00	15	08:00 – 13:00
QuikSCAT	808	21:22 – 23:04	857	07:59 – 14:49
GOES	0		525	10:02 – 12:59
GPS Dropsonde	20	18:16 – 23:48	18	08:01 – 14:28
Ship	11	18:18 – 00:00	8	08:00 – 13:00

An additional WindSat overpass of Isabel (September 14, 1040 UTC) was used for validation of wind *direction*, but it was determined that there were not sufficient observations to warrant the inclusion of that pass in the wind speed comparison.

For the two aforementioned passes, the amount of data available for each pass was sufficient for a wind speed analysis. During the WindSat overpass, both storms had an Air Force reconnaissance aircraft in the circulation taking flight-level wind measurements and releasing GPS dropwindsondes (which provide vertical profiles of several variables, including wind speed and direction from flight level to just above the surface). All wind data are transformed to a uniform 2-min average and 10-m height. The AFRES flight-level winds were reduced to 10-m wind values via a planetary boundary layer model [28]. The GOES low-level cloud drift winds were reduced through methodology developed by Dunion and Velden [23]. A plot of the data coverage for each storm is shown in Figs. 4 and 5.

B. Wind Direction Validation Set

Since a typical H*Wind analysis contains a large amount of data that lack *surface* wind direction information (e.g., AFRES flight-level winds, SFMR), surface directional analyses are found from an empirical modification of those observations. In these situations, the result is an idealized, symmetric circular flow that contains an inflow component to account for surface frictional effects. All three cases in this paper for which directional comparisons were made were represented by H*Wind as almost wholly idealized circular flows at the surface since there were very few surface wind direction observations. Thus, the wind direction validation presented in Section VI is not a comparison to an *observed* surface wind direction. However, we believe that the comparison is valid to a first approximation since surface wind flows in strong hurricanes tend to approximate idealized flows (cyclotrophic balance) very closely—at minimum over scales similar to the WindSat resolution.

V. METHODOLOGY

A. Rain Algorithm

Auxiliary TC rain fields are provided using a preliminary WindSat rain algorithm (version-0) to augment the surface wind field validation dataset. This algorithm is a modified version

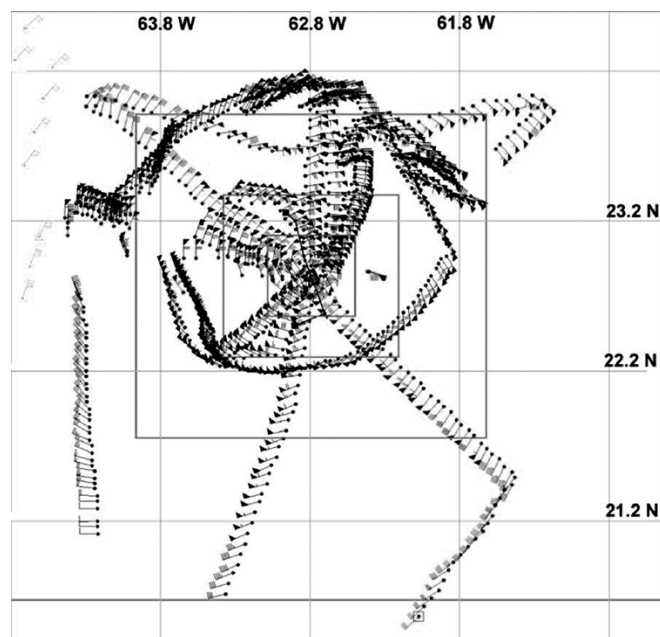


Fig. 4. Observations assimilated into the H*Wind system for Hurricane Fabian, 2147 UTC September 3. Data were collected from 1800 UTC through 0000 UTC on September 4. The location of Fabian at this time is shown as a circle in the inner box. See Table I for an expanded listing of specific data sources utilized.

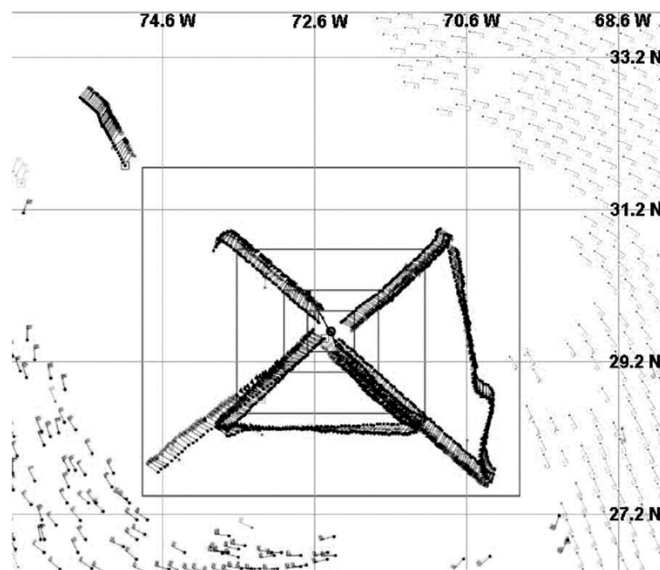


Fig. 5. Observations that were assimilated into the H*Wind system for Hurricane Isabel at 1129 UTC September 17. Data were collected from 0757 UTC through 1449 UTC. The location of Isabel at this time is shown as a circle in the inner box. See Table I for an expanded listing of specific data sources utilized.

of the Advanced Microwave Scanning Radiometer—Earth Observing System (AMSR-E) oceanic rainfall algorithm, which was originally developed at the Colorado State University [29], [30] for the Tropical Rainfall Measuring Mission (TRMM) Microwave Imager (TMI). The TMI 2A12 algorithm employs a multichannel, physically based rainfall retrieval procedure that uses cloud-resolving models to produce a large set of possible

cloud profiles (over a wide range of likely raining conditions) along with their respective passive microwave brightness temperatures. Once a database of profiles and associated brightness temperatures is established, the retrieval employs a Bayesian inversion approach to estimate rainfall on a pixel-by-pixel basis, given the set of measured brightness temperatures.

The WindSat algorithm uses four frequencies: 10.7, 18.7, 23.8, and 37 GHz. For all channels, vertically and horizontally polarized measurements are used, except for 23.8 GHz where only the vertical polarization is used. To separate the rainfall into convective and stratiform components, the AMSR-E retrieval algorithm utilizes measurements from the 37-GHz and the high-resolution 85-GHz frequency channels. Since WindSat does not have an 85-GHz channel, its algorithm depends only on the emission characteristics of the 37-GHz channel to make an assessment of the convective/stratiform nature of the rainfall.

To estimate rain rates, we use WindSat brightness temperatures resampled to every fourth 37-GHz footprint location. The rain algorithm uses forward-modeled brightness temperatures convolved with an estimate of the antenna patterns at each frequency for comparison with the measured radiances during the Bayesian inversion. The effective resolution of the rain retrievals is determined by the resolution of the cloud profile database, which is 14 km.

Preliminary validation of WindSat rain retrievals shows strong correlation with the TMI 2A12 rain rate product; however, WindSat tends to overestimate low rain rates and underestimate high rain rates [31]. Improving the WindSat algorithm rain type classification capabilities will be a major topic for future investigation. Fig. 6 provides a subjective comparison between near simultaneous WindSat and SSM/I F13 (available from Remote Sensing Systems) rain images for Hurricane Isabel. The collocation time is approximately 9 min, thereby minimizing any spatial and temporal differences between the two images. Locations of relative rain intensity agree well, allowing us to identify regions of significant rainfall, which may have an effect on wind vector retrievals.

B. Analysis Techniques

As previously discussed, the WindSat environmental data records (EDRs) are based on Tb measurements at four frequencies with up to six polarizations at each frequency (see Table II for radiometer configuration) [7]. Since each channel is of different location and resolution, the measurements must be resampled and averaged to a common size for wind vector retrieval. This analysis uses the WindSat EDR data product, version 1.5.1 processing, in which Tbs have been averaged to the 6.8-GHz footprint size and have been resampled at every fourth 37-GHz location, for a spacing of about 12.5 km.

Since H*Wind analysis files are derived at a high resolution—on the order of 6 km—we needed to convert this wind analysis to a resolution equivalent to WindSat for meaningful comparisons. Using a nearest neighbor interpolation, all H*Wind points within a radius of 25 km of the WindSat wind vector locations were weighted, inversely proportional to distance, and then averaged. Considering the inverse distance

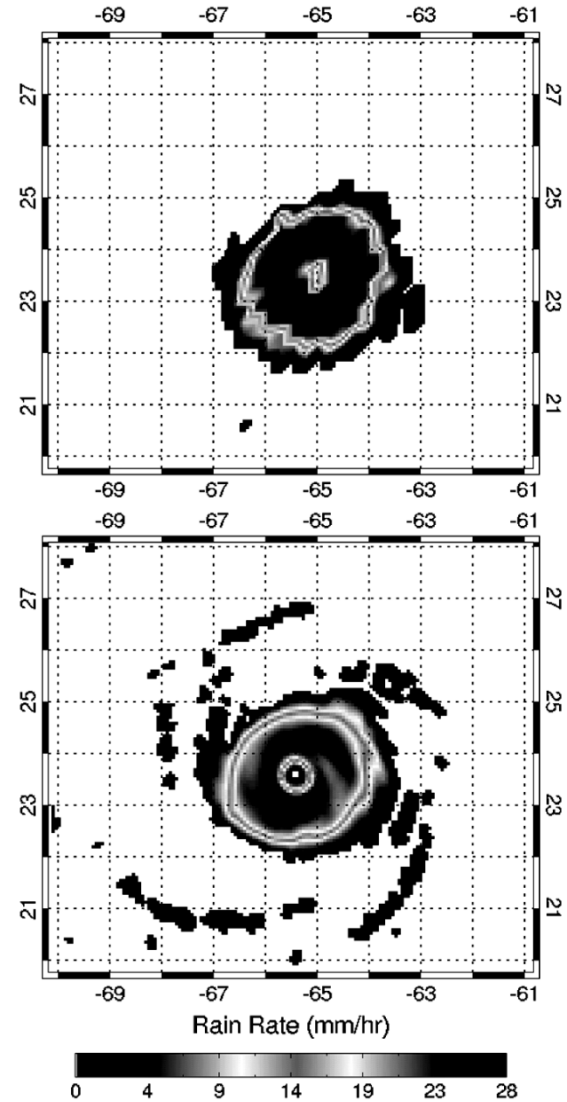


Fig. 6. Rain rates for Hurricane Isabel, September 14, morning. (Top) SSM/I 25-km resolution at 1049 UTC (see www.remss.com). (Bottom) WindSat 12.5-km resolution at 1040 UTC.

TABLE II
WINDSAT INSTRUMENT CONFIGURATION

Band, GHz	Polarization	BW, MHz	Incidence Angle, deg.	Footprint, km
6.8	V,H	125	53.5	40 x 60
10.7	V,H,+/-45,L,R	300	49.9	25 x 38
18.7	V,H,+/-45,L,R	750	55.3	16 x 27
23.8	V,H	500	53.0	12 x 20
37.0	V,H,+/-45,L,R	2000	53.0	8 x 13

weighting, this produced an effective resolution of about 25 km at the EDR spacing of approximately 12.5 km.

Customarily, within the (scatterometer) ocean vector winds scientific community, the evaluation of remotely sensed wind directions is performed globally using the “selected” wind direction alias compared with the independent “surface truth” dataset. In this manner, both the combined effect of direction retrieval accuracy and the wind direction alias selection skill are evaluated. However, for the evaluation of WindSat

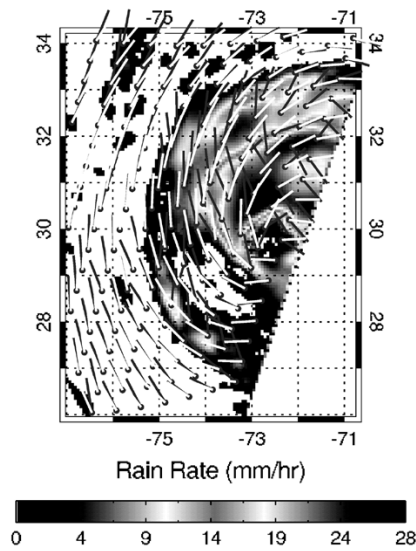


Fig. 7. Hurricane Isabel wind direction comparisons. Windsat (gray) and H*Wind (white) wind directions, September 17, 1129 UTC with WindSat rain rate background. Majority of differences are visible in the moderate to high rain areas.

directions in TCs, we choose *not to adopt this philosophy* and will evaluate the accuracy of the “closest” WindSat wind alias to the H*Wind direction. Considering the immaturity of the WindSat version-0 geophysical model function, especially for high winds and a highly attenuating atmosphere environment in TCs, we believe that it is unfair to penalize the wind direction measurement accuracy based upon poor wind alias selection skill. A note should be made that we are evaluating the best case scenario. Thus, direction retrievals may not reach the level of accuracy of the closest alias, due to limitations in alias selection.

The H*Wind surface wind analysis typically covers a region of $\pm 400\text{--}500$ km surrounding the hurricane center, and wind direction differences are calculated at each EDR location. For the wind direction evaluation, we define WindSat retrieval direction differences as “closest” WindSat direction minus the corresponding H*Wind direction. The relative azimuth, χ , is defined as wind direction minus the WindSat antenna azimuth look direction, where $\chi = 0^\circ$ is a wind blowing toward the antenna.

C. WindSat Hurricane Passes

Three Atlantic hurricanes are used for this anecdotal case study. As discussed in Section IV, two are chosen because of the availability of coincident aircraft measurements of surface winds at the time of the WindSat pass. The selected storms are Fabian (September 3, 2003 2147 UTC) and Isabel (September 17, 2003 1129 UTC), for which a wind speed and directional analysis is performed. A third pass, Isabel on September 14, 1040 UTC, is also used for directional analysis. Because of the lack of sufficient wind speed data near this time, the magnitude of the wind vectors was not considered for this pass. As discussed in Section IV, this does not preclude a feasible directional analysis.

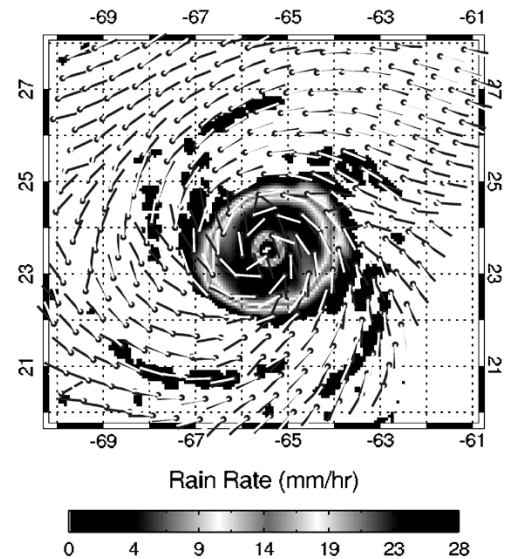


Fig. 8. Hurricane Isabel wind direction comparisons. WindSat (gray) and H*Wind time interpolated (white) wind directions, September 14, 1040 UTC with WindSat rain rate background. Large differences are present northeast and northwest of the eye outside of the raining region.

VI. RESULTS

A. Wind Directions

Subjective evaluations of WindSat wind flow patterns are made by examining both the WindSat and H*Wind images for the three hurricane cases described above, given in Figs. 7–9. In each image, the wind direction is shown as a unit length vector with the WindSat closest direction shown in gray and the H*Wind analysis direction shown in magenta. For clarity of presentation, the EDRs have been thinned with only about 25% of the locations plotted. Also the WindSat rain rate is plotted as a grayscale background with rain rates of 0 mm/h shown in white.

Fig. 7 shows the wind comparisons for the Isabel pass on September 17, 1129 UTC. It should be noted that wind retrievals are performed in all regions of the storm. This has not been the case for conventional microwave radiometer retrieval algorithms, which have been designed to retrieve only rain when rain is present. Thus, it is apparent that third and fourth Stokes parameters exist even in the presence of rain; but the question is “Are the retrievals sensible?” In this example, there is generally good agreement between the flow patterns of WindSat and H*Winds for wind directions outside areas of intense rain. However, within the rain areas, there are apparent systematic differences in the wind directions. By closer visual inspection, the direction differences are much greater in the raining regions, especially those areas with moderate to high rains. This same behavior is apparent for WindSat’s pass over Isabel on September 14, shown in Fig. 8. Wind directions within the moderate to high rain areas display large differences; additionally, there appears to be a systematic problem in the western region of the storm, outside of any rain. This behavior is even more obvious in Hurricane Fabian on September 3 (Fig. 9), where, we find large systematic differences in the rain-free regions east and southeast of the center. In general, the WindSat directional retrievals in those

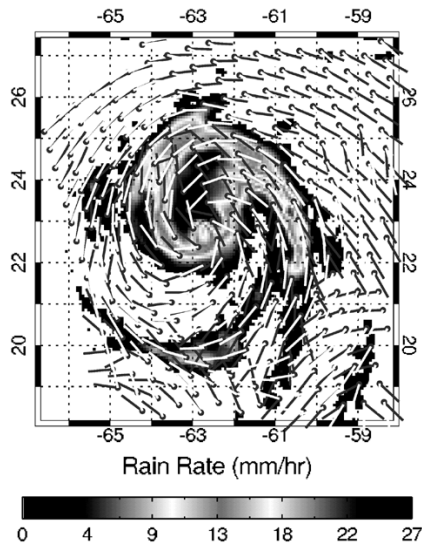


Fig. 9. Hurricane Fabian wind direction comparisons. WindSat (gray) and H*Wind (white) wind directions, September 3, 2147 UTC with WindSat rain rate background. Large differences are present east and southeast of the eye outside of the raining region.

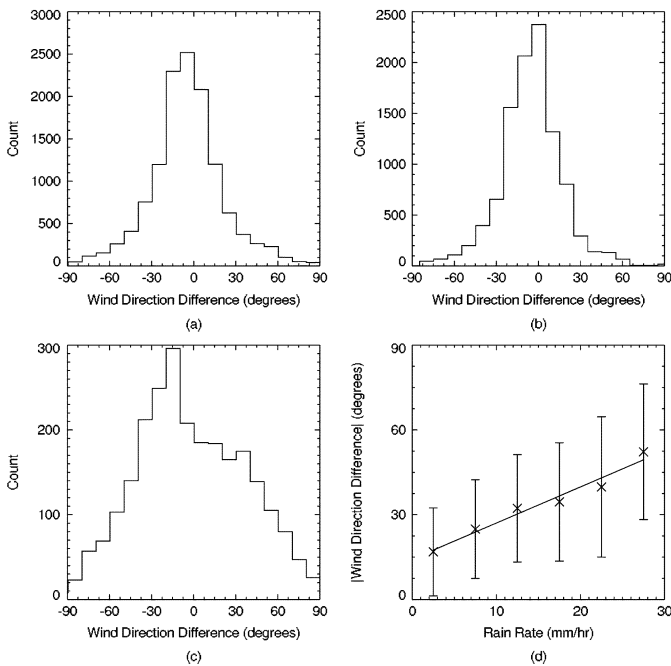


Fig. 10. Wind direction statistical analysis of overall WindSat performance for three hurricane passes from 2003 hurricane season. (a) Wind direction difference for all data. (b) Corresponds to rain rates less than 4 mm/h. (c) Wind direction difference for rain rates above 4 mm/h. (d) Shows a strong linear correlation between the magnitude of the wind direction difference and rain rates. Xs are absolute mean direction difference, with vertical lines denoting standard deviation of each bin. Linear fit to the data is also plotted.

areas are not physically realizable. Also, as expected, wind directions are highly erroneous in rain regions.

A quantitative evaluation is presented in Fig. 10, which shows a composite statistical analysis of the three hurricanes mentioned previously. For all data [Fig. 10(a)] there is a slight bias of -4.3° and the RMS difference of 25.7° , which is consistent with the expected global performance of WindSat wind direction retrievals. This result is somewhat misleading because the

TABLE III
WIND DIRECTION ERROR STATISTICS

		Fabian	Isabel 09/14	Isabel 09/17	All
All Data	Mean	-6.3	-4.07	-1.27	-4.27
	STD	30.01	20.35	25.73	25.73
	Num Obs	5009	4805	2939	12753
Rain < 4 mm/hr	Mean	-8.79	-3.01	-0.19	-4.7
	STD	27.28	17.71	16.38	21.99
	Num Obs	1333	820	1335	3488
Rain > 4 mm/hr	Mean	7.01	-13.44	-3.81	-2.17
	STD	39.07	34.71	39.78	39.17
	Num Obs	3676	3985	1604	9265

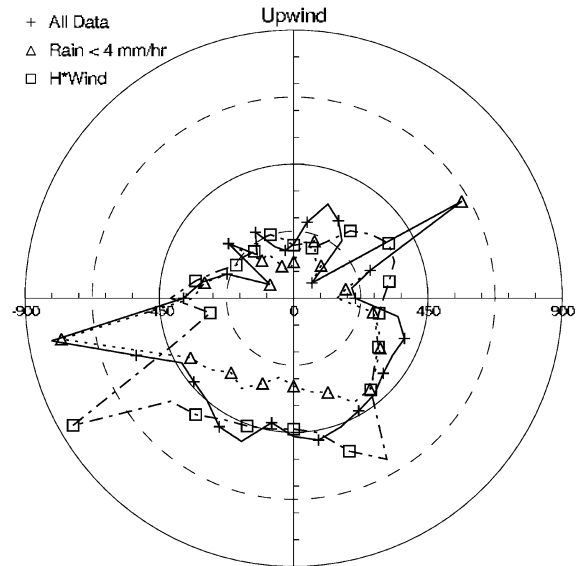


Fig. 11. Relative wind direction polar histogram for closest wind direction aliases and H*Wind directions.

hurricane force winds and the moderate to high rain rates occupy only about 10% of the total comparison region; so the majority of points are outside of this difficult region. In Fig. 10(b), only locations where the rain rate below 4 mm/h are included, and the RMS difference decreases to 22.0° . In Fig. 10(c), wind direction retrievals are significantly affected by the presence of rain rates over 4 mm/h, with differences in these high rain regions being 39.2° . In particular, results shown in Fig. 10(d), a scatter diagram of the RMS wind direction difference versus rain rate, exhibit a strong linear correlation. Detailed statistics are available in Table III.

While the histograms described above show good results for wind directional retrievals for nonraining regions, there are other statistical metrics presented in Fig. 11, which indicate probable deficiencies in the model function. In the wind direction algorithm, solutions are found in terms of the relative wind direction χ , and then from the measurement geometry (antenna azimuth relative to north), the wind direction is calculated. Insight can be found by examining relative differences between

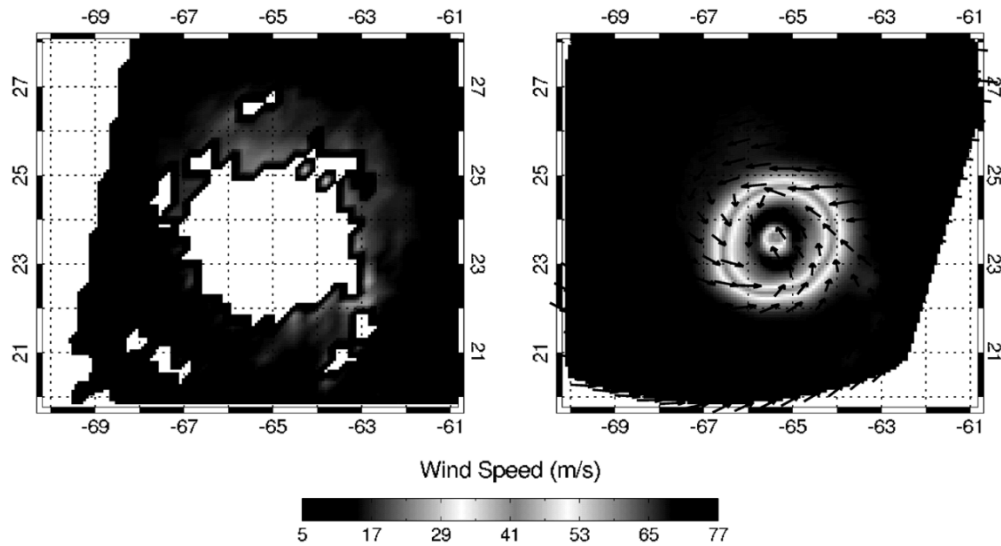


Fig. 12. (Left) SSM/I wind speed retrieval (see www.remss.com) and (right) WindSat wind field. Hurricane Isabel, September 14, 1040 UTC.

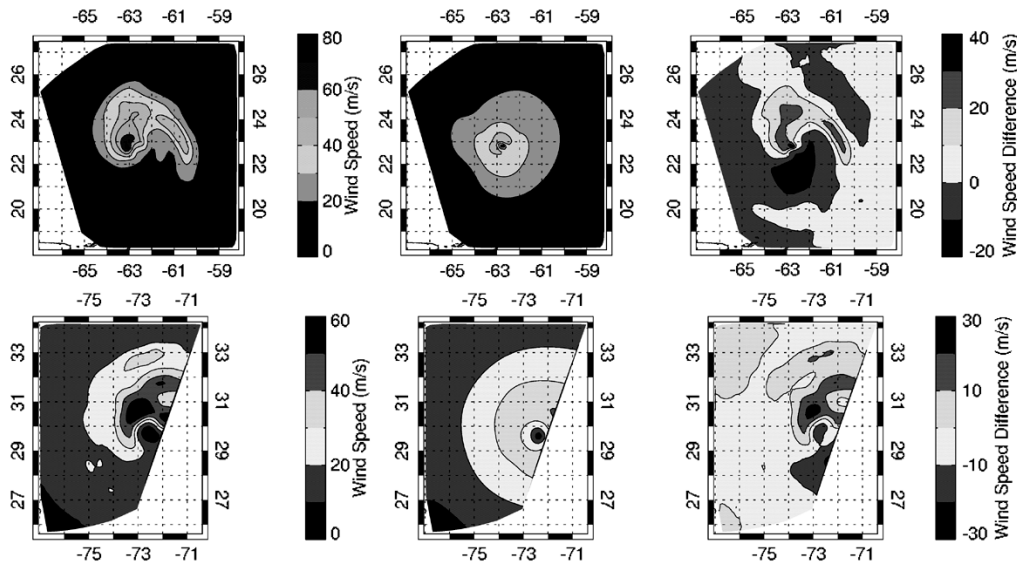


Fig. 13. Hurricane wind speed comparison. (Top) Fabian, September 3, 2147 UTC. (Bottom) Isabel, September 17, 1129 UTC. (Left) WindSat wind speeds. (Middle) H*Wind. (Right) Wind speed difference. Contours are in steps of 10 m/s.

the distribution of relative directions from: 1) the measurement geometry and the independent estimates of wind directions and 2) the closest retrieved χ . Such polar plots are presented in Fig. 11 showing the relative wind direction histograms for the H*Wind directions and for the closest WindSat aliases. It is noted that there are “spikes” in the WindSat distribution, which are indicative of the algorithm “locking-in” to certain preferred directions. However, similar features are not observed in the H*Winds histogram. Experience in the scatterometer ocean vector wind science community has shown that such histogram anomalies are excellent indicators of problems associated with the geophysical model function [32]. Because these spikes appear both in the all data (including rain) and nonrain histograms, it is believed that they are not the result of rain; rather they are probably the result of an improper anisotropy signature of the third and fourth Stokes GMF.

B. Wind Speeds Versus H*Wind

Radiometric wind speed retrievals in a hurricane environment are severely disadvantaged considering that the WindSat geophysical model function has not been fully developed for wind speeds above 20 m/s, nor have the effects of rain been included in algorithm development. Unlike the wind directions, WindSat retrievals of wind magnitudes are quite poor over the majority of the hurricane area. Since the wind speed retrieval uses the conventional (nonpolarimetric) channels, one would expect similar results as the heritage SSM/I algorithm (see Fig. 12). Note that the SSM/I wind retrieval algorithm does not retrieve wind speeds in the region of moderate to high rain. For WindSat, the presence of rain overpowers the measured Tbs, and the resulting wind retrievals have large residuals of rain in them.

This can be seen in wind contour comparisons of WindSat retrievals and H*Wind wind speeds shown in Fig. 13. The

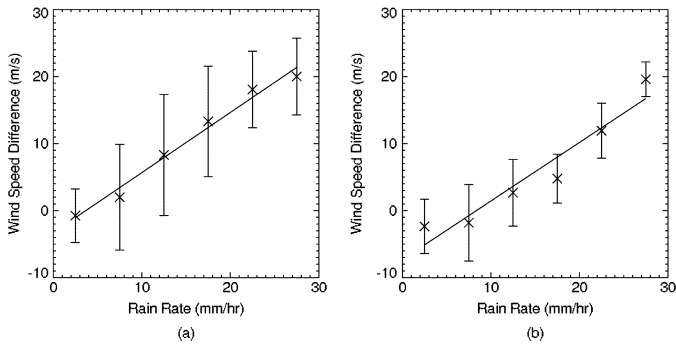


Fig. 14. Hurricane wind speed difference versus rain rate. (a) Fabian, September 3, 2147 UTC. (b) Isabel, September 17, 1129 UTC. Xs are mean wind speed differences for 5-mm/h rain bins, and vertical lines denote standard deviations. Linear fit is also plotted.

WindSat wind speed difference contours shown in the lower panel strongly resemble the rain map. Fig. 13 shows the WindSat wind speed (left), H*Wind wind speed analysis (middle), and the difference between the two (right, WindSat—H*Wind) for Hurricane Fabian (top, September 3, 2147 UTC) and Hurricane Isabel (bottom, September 17, 1129 UTC). This figure immediately suggests that heavy rainfall is overwhelming any surface signal in the core and rain band areas of the TCs. For the Fabian case, WindSat maximum retrieved winds exceed 70 m/s—far higher than the official intensity estimate provided by the NHC near that time (55 m/s at 1800 UTC and 57.5 m/s at September 4, 0000 UTC). When AFRES data are available, the NHC intensities are determined primarily from flight-level winds and are generally considered reliable.

Furthermore, both cases feature a wind speed difference pattern that is spatially correlated to a large degree with areas of heavy rain (see Figs. 7 and 9 for comparison). For example, differences of 20–30 m/s in the Fabian pass (Fig. 13, top right image) are found near 23°N 83°W—collocated with a large area of 27+ mm/h rainfall (Fig. 9). Rain band patterns are clearly evident as well in both cases. Curiously, a large negative bias area is found to the south and southeast of each system. Although an exact cause cannot be determined with any certainty, we point out that rain is light or absent in those areas. Fig. 14 reveals a strong relationship between rain rate and the wind speed difference—both show increasing wind speed difference with increasing rain rate. It is also certainly possible that the H*Wind analysis is not as accurate in that region due to a lower density of observations there.

C. WindSat Wind Speed Versus Surface Observations

Given the uncertainties and possible errors in the H*Wind analyses, we have also performed a comparison of WindSat wind speeds with various surface observations, both *in situ* and remotely sensed. We considered a point observation to be collocated if it was taken within 10 km and 40 min of the WindSat overpass time.

Table IV shows the results from the analysis. H*Wind statistics, which are calculated from an analysis that already incorporates all of the other surface data, are included for compar-

TABLE IV
STATISTICS FROM WINDSAT COLLOCATIONS WITH VARIOUS SURFACE WIND SPEED OBSERVATIONS. UNITS ARE METERS PER SECOND

	Buoy		Ship	SFMR	QuikSCAT			H*Wind	
Storm	Isabel			Fabian	Isabel	Fabian	Isabel	Fabian	Isabel
Bias	-1.12	0.22	5.75	N/A	-1.37	-2.71	0.10	0.38	
Std. Dev.	0.86	0.57	10.38	N/A	0.54	0.97	6.33	6.15	
RMSE	1.40	0.56	11.85	N/A	1.47	2.88	6.33	6.16	
R ²	0.87	0.99	0.08	N/A	0.93	0.95	0.64	0.68	
n	48	6	248	N/A	165	474	2048	1424	

ison purposes. There is very good agreement between WindSat wind speeds and buoy, ship, and QuikSCAT observations with biases and root mean square (RMSE) errors generally less than 2 m/s. This is an encouraging result, but one should keep in mind that all of the buoy, ship, and QuikSCAT data are taken from areas outside of the TC core and are not indicative of a high wind/heavy rain environment (rain-flagged QuikSCAT winds were not included).

We look to the SFMR data for an indication of WindSat wind speed quality near the TC core, where high rain rates and cloud liquid water content present a big challenge. For the Fabian pass, there is a high bias (5.75 m/s) and variability in the WindSat data with almost zero correlation to the SFMR data. With the caveat that this is only one pass, this result combined with the H*Wind comparison presented above give little confidence in the WindSat wind speeds in heavy rain at this time.

There are other observations from GPS dropwindsonde surface measurements near the TC core (excluding eye drops). For the Fabian (Isabel) pass, the WindSat bias is 3.63 (11.96) m/s with a root mean square error of 4.18 (17.75) m/s. However, there are only three collocations for the Fabian pass and two for the Isabel pass. In addition, they are point measurements taken in a highly temporally and spatially variable wind environment, up to 30 min separate from the WindSat pass time. Thus, these results should not be considered completely reliable, but they do support the other surface data in suggesting a high bias in WindSat retrievals in rainy regions near the TC core.

D. Wind Speed Comparison Summary

More WindSat passes over TCs must be reviewed to determine if this is a persistent pattern in the retrievals. Around the periphery of each system, there is a larger degree of agreement between WindSat and the H*Wind analysis, particularly within the wind speed range of 10–20 m/s. However, if the egregious differences seen in these two cases are evident in other cases, WindSat surface wind speed retrievals will not be usable in the rainy area of TCs, unless suitable correction algorithms can be developed.

VII. CONCLUSION

This paper evaluates WindSat wind vector performance in a few year–2003 Atlantic hurricanes by comparison with independent surface wind field estimates using the H*Wind software analysis tool. Unfortunately, for hurricanes, there is no realiz-

able “surface truth”; but H*Wind provides a useful tool for compositing a rather diverse collection of spatially and temporally distributed estimates of surface wind magnitude and a few directions. So with all of its limitations, H*Wind is the best that is available; and even though the WindSat comparisons are largely qualitative, they are nonetheless very useful.

The comparison results for wind speeds demonstrate that the version-0 algorithm does not perform well. This is not a surprise, because it was never intended to. This algorithm was developed for “nonprecipitating atmospheres and at ocean surface winds less than 20 m/s.” The vertically and horizontally polarized Tbs are strongly affected by heavy cloud cover and precipitation in and around TCs; so it is doubtful that the wind speed retrieval will ever improve. However, the fact that the third and fourth Stokes signals exist in this environment provides hope that a new algorithm might be developed to retrieve both wind speed and direction from these parameters.

Concerning wind directions, the comparisons are better. The magnitude of the third and fourth Stokes anisotropic signal increases with wind speed, which helps. Outside of the immediate vicinity of the hurricanes, the wind flow patterns look believable, except for a few regions where the WindSat retrieval and H*Wind diverge. The reasons for this are not understood; but since the wind direction algorithm uses “bogus” WindSat wind speed retrievals, this may influence the results. This needs further investigation. Within a few hundred kilometers of the storm center, at locations with precipitation below 4 mm/h (as inferred by an experimental WindSat rain algorithm), the wind direction differences increase with rain rate. This is clearly a failure of the algorithm; nevertheless there are some successes where believable wind direction retrievals are made between the intense spiral rain bands, even in regions of heavy clouds.

Finally, a few comments should be made to put Windsat wind retrievals in hurricanes into proper perspective. Despite the less than desired performance, the authors are encouraged with the limited successes. We feel that future developments, aimed at wind vector retrievals in hurricanes, such as including hurricane force winds into the empirical model function and understanding the effects of rain on the polarimetric channels, will likely improve retrievals. Additionally, using the polarimetric information to retrieve wind speed should improve retrievals for both magnitude and direction. After all, the scatterometer remote sensing community has been investigating this special application for decades with only limited success—it is a really tough problem that requires persistence and innovative approaches to advance.

ACKNOWLEDGMENT

The authors would like to thank R. Knabb (Tropical Prediction Center) for reviewing the manuscript and M. Powell (Hurricane Research Division) for clarifying many H*Wind issues and questions. Many thanks to C. Kummerow for help in applying the AMSR-E rain algorithm to WindSat.

REFERENCES

- [1] R. K. Moore and W. L. Jones, “Satellite scatterometer wind vector measurement—The legacy of the Seasat satellite scatterometer,” *IEEE Geosci. Remote Sens. Newsl.*, no. 321, Sep. 2004.
- [2] J. P. Hollinger, J. L. Peirce, and G. A. Poe, “SSM/I instrument evaluation,” *IEEE Trans. Geosci. Remote Sens.*, vol. 28, no. 5, pp. 781–790, Sep. 1990.
- [3] M. A. Goodberlet, C. T. Swift, and J. C. Wilkerson, “Ocean surface wind speed measurements of the Special Sensor Microwave/Imager (SSM/I),” *IEEE Trans. Geosci. Remote Sens.*, vol. 28, no. 5, pp. 823–828, Sep. 1990.
- [4] F. J. Wentz, “Measurement of oceanic wind vector using satellite microwave radiometers,” *IEEE Trans. Geosci. Remote Sens.*, vol. 30, no. 5, pp. 960–972, Sep. 1992.
- [5] P. S. Chang and L. Li, “Ocean surface wind speed and direction retrievals from the SSM/I,” *IEEE Trans. Geosci. Remote Sens.*, vol. 36, no. 6, pp. 1866–1871, Nov. 1998.
- [6] Z. Jelenak, private communication.
- [7] Z. Jelenak, T. Mavor, L. Connor, N.-Y. Wang, P. S. Chang, and P. Gaiser, “Validation of ocean wind vector retrievals from WindSat polarimetric measurements,” presented at the *4th Int. Asian-Pacific Environmental Remote Sensing Conf.*, 2004.
- [8] L. N. Connor, P. S. Chang, Z. Jelenak, N.-Y. Wang, and T. P. Mavor, “WindSat validation datasets: An overview,” in *Proc. IGARSS*, vol. 1, Sep. 2004, pp. 386–389.
- [9] D. E. Weissman, M. A. Bourassa, J. J. O’Brien, and J. S. Tongue, “Calibrating and validating the QuikSCAT/SeaWinds radar for measuring rain rate over the ocean,” *IEEE Trans. Geosci. Remote Sens.*, vol. 41, no. 12, pp. 2814–2820, Dec. 2003.
- [10] W. L. Jones, V. J. Cardone, W. J. Pierson, J. Zec, L. P. Rice, A. Cox, and W. B. Sylvester, “NSCAT high resolution surface winds measurements in typhoon violet,” *J. Geophys. Res.*, vol. 104, no. C5, May 1999.
- [11] W. L. Jones and J. Zec, “Evaluation of Rain Effects on NSCAT Wind Retrievals,” presented at the *Oceans 96 Conf.*, Ft. Lauderdale, FL, Sep. 23–26, 1996.
- [12] F. J. Wentz, “A well-calibrated ocean algorithm for SSM/I,” *J. Geophys. Res.*, vol. 102, pp. 8703–8718, 1997.
- [13] P. W. Gaiser *et al.*, “The Windsat spaceborne polarimetric microwave radiometer: Sensor description and early orbit performance,” *IEEE Trans. Geosci. Remote Sens.*, vol. 42, no. 11, pp. 2347–2361, Nov. 2004.
- [14] S. H. Yueh, W. J. Wilson, F. K. Li, W. B. Ricketts, and S. V. Nghiem, “Polarimetric brightness temperatures of sea surfaces measured with aircraft K- and Ka-band radiometers,” *IEEE Trans. Geosci. Remote Sens.*, vol. 33, no. 5, pp. 1177–1187, Sep. 1997.
- [15] S. H. Yueh, W. J. Wilson, S. J. DiNardo, and F. K. Li, “Polarimetric microwave brightness signatures of ocean wind direction,” *IEEE Trans. Geosci. Remote Sens.*, vol. 37, no. 2, pp. 949–959, Mar. 1999.
- [16] P. S. Chang, P. W. Gaiser, L. Li, and K. M. St. Germain, “Multi-frequency polarimetric microwave ocean wind direction retrievals,” in *Proc. IGARSS*, vol. 2, Singapore, Aug. 1997, pp. 1009–1011.
- [17] J. R. Piepmeier and A. J. Gasiewski, “High-resolution passive polarimetric microwave mapping of the ocean surface wind vector fields,” *IEEE Trans. Geosci. Remote Sens.*, vol. 39, no. 3, pp. 606–622, Mar. 2001.
- [18] G. A. Wick, J. J. Bates, and C. C. Gottschall, “Observational evidence of a wind direction signal in SSM/I passive microwave data,” *IEEE Trans. Geosci. Remote Sens.*, vol. 38, no. 2, pp. 823–837, Mar. 2000.
- [19] K. M. St. Germain, G. A. Poe, and P. W. Gaiser, “Polarimetric emission model of the sea at microwave frequencies and comparison with measurements,” *Progr. Electromag. Res.*, vol. 37, pp. 2–32, 2002.
- [20] L. Tsang, J. A. Kong, and R. T. Shin, *Theory of Microwave Remote Sensing*. New York: Wiley, 1985.
- [21] M. D. Powell, S. H. Houston, L. R. Amat, and N. Morisseau-Leroy, “The HRD real-time hurricane wind analysis system,” *J. Wind Eng. Indust. Aerodynam.*, vol. 77 & 78, pp. 53–64, 1998.
- [22] E. W. Uhlhorn and P. G. Black, “Verification of remotely sensed sea surface winds in hurricanes,” *J. Atmos. Oceanic Technol.*, vol. 20, pp. 99–116, 2003.
- [23] J. P. Dunion and C. S. Velden, “Application of surface-adjusted GOES low-level cloud-drift winds in the environment of Atlantic tropical cyclones. Part I: Methodology and validation,” *Mon. Weather Rev.*, vol. 140, pp. 1333–1346, 2002.
- [24] J. L. Franklin, M. L. Black, and K. Valde, “GPS dropwindsonde wind profiles in hurricanes and their operational implications,” *Weather Forecast.*, vol. 18, pp. 32–44.
- [25] A. Bentamy, E. Autret, P. Queffelec, and Y. Quilfen, “Intercomparison of ERS-2 and QuikSCAT winds,” in *Proc. IGARSS*, vol. 1, Jul. 24–29, 2005, pp. 269–271.
- [26] J. L. Franklin, private communication.

- [27] S. H. Houston, W. A. Shaffer, M. D. Powell, and J. Chen, "Comparisons of HRD and SLOSH surface wind fields in hurricanes: Implications for storm surge modeling," *Weather Forecast.*, vol. 14, pp. 671–686, 1999.
- [28] M. D. Powell, "Evaluations of diagnostic marine boundary-layer models applied to hurricanes," *Mon. Weather Rev.*, vol. 108, pp. 757–766, 1980.
- [29] C. Kummerow, W. Olson, and L. Giglio, "A simplified scheme for obtaining precipitation and vertical hydrometeor profiles from passive microwave sensors," *IEEE Trans. Geosci. Remote Sens.*, vol. 34, no. 5, pp. 1213–1232, Sep. 1996.
- [30] T. Wilheit, C. Kummerow, and R. Ferraro, "Algorithm Theoretical Basis Document for EOS/AMSR rainfall," Texas A&M Univ., College Park, TX, 1999.
- [31] K. Ahmad, W. L. Jones, J. Thomas-Stahle, and C. Kummerow, "Oceanic rain rates from the WindSat radiometer," in *Proc. IGARSS*, Jul. 2005, pp. 25–29.
- [32] N. Ebuchi, "Statistical distribution of wind speeds and directions globally observed by NSCAT," *J. Geophys. Res.*, vol. 1041, no. C5, pp. 11 393–11 43, May 1990.

Ian S. Adams (S'01) received the B.S.E.E. and M.S.E.E. degrees from the University of Central Florida (UCF), Orlando, in 2001 and 2005, respectively. He is currently pursuing the Ph.D. degree in electrical engineering at UCF.

From 2000 to 2005, he worked at the Central Florida Remote Sensing Laboratory, UCF, where his primary research was in the development of an hurricane wind speed retrieval algorithm for the SeaWinds Scatterometer. He is currently working at the Naval Research Laboratory, Washington, DC, where he is investigating the effects of rain on polarimetric radiometer retrievals. His research interests include active and passive remote sensing retrieval algorithm development and the remote sensing of tropical cyclones.

Mr. Adams is a student member of the American Geophysical Union.

Christopher C. Hennon received the B.A. degree in aeronautics from Miami University, Miami, OH, the M.S. degree in atmospheric science from Purdue University, West Lafayette, IN, and the Ph.D. degree in atmospheric science (specializing in tropical meteorology) from The Ohio State University, Columbus, in 1994, 1996, and 2003, respectively.

He worked as a University Corporation for Atmospheric Research Postdoctoral Fellow and Visiting Scientist at the Tropical Prediction Center, Miami, FL from 2003 to 2005. Currently, he is an Assistant Professor of atmospheric sciences at the University of North Carolina, Asheville. His research interests include tropical cyclogenesis, statistical modeling, and weather forecasting.

Dr. Hennon is a member of the American Meteorological Society and the American Geophysical Union.



W. Linwood Jones (SM'75–F'99) received the B.S. degree from the Virginia Polytechnic Institute, Blacksburg, the M.E.E. degree from the University of Virginia, Charlottesville, and the Ph.D. degree from the Virginia Polytechnic Institute and State University, in 1962, 1965, and 1971, respectively, all in electrical engineering.

He has over 30 years professional experience with the National Aeronautics and Space Administration (NASA)—Langley Research Center 1962–1981; NASA Headquarters 1988–1992; and the Kennedy Space Center 1992–1994—and the private aerospace industry—GE Space Division, King of Prussia, PA 1981–1982; Satellite TV Corp., Hightstown, NJ 1982–1984; and Harris Corp., Melbourne, FL 1984–1988. Also, he has over ten years experience in college academia—Florida Institute of Technology, Melbourne, 1994–1996 and the University of Central Florida (UCF), Orlando, 1996–present. At UCF, he is a Professor in the Electrical and Computer Engineering Department, where he teaches undergraduate and graduate courses in satellite communications and remote sensing, and radar systems. Also, he is the Director of the Central Florida Remote Sensing Laboratory, where he performs research in satellite microwave remote sensing. He is a member of the science teams for the Jet Propulsion Laboratory's SeaWinds Scatterometer Program, the NASA Goddard Space Flight Center's Precipitation Measuring Mission, and the Naval Research Laboratory's WindSat Mission.

Dr. Jones is a member of the Union of Radio Scientists International, Commission-F, the American Geophysical Union, the IEEE Geoscience and Remote Sensing Society, the IEEE Antennas and Propagation Society, and the IEEE Ocean Engineering Society.



Khalil A. Ahmad (S'01) received the B.S. degree in electronics engineering from Princess Sumaya University, Amman, Jordan, and the M.S.E.E. degree from the University of Central Florida, Orlando (UCF), in 1999 and 2004, respectively. He is currently pursuing the Ph.D. degree in electrical engineering at UCF.

He joined the Central Florida Remote Sensing Laboratory, UCF in fall 2001, where he has been working on remote sensing of oceanic rain using satellite data. His research interests include active and passive microwave remote sensing retrieval algorithm development and signal processing.